

## Communication

**Gate-tunable Giant Stark Effect in Few-layer Black Phosphorus**

Yanpeng Liu, Zhizhan Qiu, Alexandra Carvalho, Yang Bao, Hai Xu, Sherman Jun Rong Tan, Wei Liu, Antonio H. Castro Neto, Kian Ping Loh, and Jiong Lu

*Nano Lett.*, **Just Accepted Manuscript** • DOI: 10.1021/acs.nanolett.6b05381 • Publication Date (Web): 14 Feb 2017

Downloaded from <http://pubs.acs.org> on February 15, 2017

**Just Accepted**

“Just Accepted” manuscripts have been peer-reviewed and accepted for publication. They are posted online prior to technical editing, formatting for publication and author proofing. The American Chemical Society provides “Just Accepted” as a free service to the research community to expedite the dissemination of scientific material as soon as possible after acceptance. “Just Accepted” manuscripts appear in full in PDF format accompanied by an HTML abstract. “Just Accepted” manuscripts have been fully peer reviewed, but should not be considered the official version of record. They are accessible to all readers and citable by the Digital Object Identifier (DOI®). “Just Accepted” is an optional service offered to authors. Therefore, the “Just Accepted” Web site may not include all articles that will be published in the journal. After a manuscript is technically edited and formatted, it will be removed from the “Just Accepted” Web site and published as an ASAP article. Note that technical editing may introduce minor changes to the manuscript text and/or graphics which could affect content, and all legal disclaimers and ethical guidelines that apply to the journal pertain. ACS cannot be held responsible for errors or consequences arising from the use of information contained in these “Just Accepted” manuscripts.



# Gate-tunable Giant Stark Effect in Few-layer Black Phosphorus

Yanpeng Liu<sup>1,2,γ</sup>, Zhizhan Qiu<sup>1,3,γ</sup>, Alexandra Carvalho<sup>2,4,γ</sup>, Yang Bao<sup>1,2</sup>, Hai Xu<sup>1,2</sup>, Sherman J. R. Tan<sup>1,3</sup>, Wei Liu<sup>1,2</sup>, A. H. Castro Neto<sup>2,4</sup>, Kian Ping Loh<sup>1,2,\*</sup> and Jiong Lu<sup>1,2,\*</sup>

<sup>1</sup>Department of Chemistry, National University of Singapore, 3 Science Drive 3, Singapore 117543

<sup>2</sup>Centre for Advanced 2D Materials and Graphene Research Centre, National University of Singapore, Singapore 117546

<sup>3</sup>NUS Graduate School for Integrative Sciences and Engineering, National University of Singapore, 28 Medical Drive, Singapore 117456

<sup>4</sup>Department of Physics, National University of Singapore, 3 Science Drive 2, Singapore 117542

\*Email: [chmlhkp@nus.edu.sg](mailto:chmlhkp@nus.edu.sg) (K.P.L.); [chmluj@nus.edu.sg](mailto:chmluj@nus.edu.sg) (J.L.)

## Abstract:

Two-dimensional black phosphorus (BP) has sparked enormous research interest due to its high carrier mobility, layer-dependent direct bandgap and outstanding in-plane anisotropic properties. BP is one of the few two-dimensional materials where it is possible to tune the bandgap over a wide energy range from the visible up to the infrared. In this article, we report the observation of a giant Stark effect in electrostatically-gated few-layer BP. Using low temperature scanning tunnelling microscopy, we observed that in few-layer BP, when electrons are injected, a monotonic reduction of the bandgap occurs. The injected electrons compensate the existing defect-induced holes and achieve up to 35.5% bandgap modulation in the light-doping regime. The local density of states in few-layer BP, when probed by tunnelling spectroscopy, shows characteristic resonance features arising from layer-dependent sub-band structures due to

1  
2  
3  
4 25 quantum confinement effects. The demonstration of an electrical gate-controlled giant Stark  
5  
6 26 effect in BP paves the way to designing electro-optic modulators and photodetector devices that  
7  
8 27 can be operated in a wide electromagnetic spectral range.  
9

10  
11 28 **Keywords:** *Black phosphorus, Giant Stark effect, bandgap, electrostatical-gating, scanning*  
12  
13 29 *tunnelling microscopy*  
14

15  
16  
17 30 **TEXT**  
18

19  
20 31 The Stark effect is the shifting and splitting of atomic energy levels under the influence of  
21  
22 32 an externally applied electric field. In semiconductors, in the presence of an electric field, the  
23  
24 33 Stark effect will cause the energy levels to shift, which in turn modifies the bandgap. Hence, by  
25  
26 34 changing the electric field, the electro-optical response of the material can be tuned.<sup>1,2</sup> In  
27  
28 35 quantum-confined systems, the Stark effect often gives a strong optical bandgap modulation due  
29  
30 36 to inhibited exciton field ionization and reduced field screening as opposed to that in bulk  
31  
32 37 materials.<sup>3,4</sup> The quantum-confined Stark effect (QCSE) is the basis on which III-V  
33  
34 38 semiconductor-based optical modulators operate.<sup>3</sup> However, the relatively low energy offset  
35  
36 39 between the quantized transitions and the surrounding cladding (such as GaAs, with a bandgap  
37  
38 40  $\sim 1.52$  eV at 4K) means that even operational fields greater than only a few tens of  $\text{kV cm}^{-1}$  can  
39  
40 41 cause the tunnelling-out of the electrons to occur.<sup>4</sup> Some two dimensional (2D) materials can  
41  
42 42 potentially show a stronger Stark effect beyond those encountered in quantum-well structures  
43  
44 43 due to its weaker dielectric screening, and its strongly anisotropic properties. However, it is  
45  
46 44 difficult to induce a semiconductor-to-metal transition in bilayer transition metal dichalcogenides  
47  
48 45 (TMDs) by tuning the externally applied electric field because of the relatively large bandgap  
49  
50  
51  
52  
53  
54  
55  
56  
57  
58  
59  
60

1  
2  
3  
4 46 (! 1eV) of these materials, the critical external electric field for such a transition being in the  
5  
6 47 range 2–3 V/nm.<sup>5</sup>  
7

8  
9 48 Black phosphorus (BP), a layered allotropic form of elemental phosphorus, has attracted  
10  
11 49 increased attention from researchers because of its layer-dependent bandgap spanning the entire  
12  
13 50 electromagnetic spectrum, which is unmatched by any other 2D material known to date.<sup>6-12</sup> BP  
14  
15 51 has both high mobility and a thickness-dependent direct bandgap (~2.0 eV for monolayer and  
16  
17 52 ~0.3 eV for bulk sample owing to the strong interlayer coupling).<sup>12-14</sup> In view of its  
18  
19 53 orthorhombic crystal lattice with a puckered honeycomb structure, the conduction band  
20  
21 54 minimum (CBM) and the valence band maximum (VBM) of BP are mainly contributed by  
22  
23 55 localized P 3p<sub>z</sub> orbitals (vertical to the puckered plane) rather than by 3p<sub>x</sub> and 3p<sub>y</sub>, which means  
24  
25 56 that the electronic properties of BP are very sensitive to electric field applied perpendicularly.<sup>15</sup>  
26  
27 57 The Stark effect coefficient is a parameter which reflects the rate of the reduction of band gap  
28  
29 58 with applied field strength. The small bandgap (~0.3 eV in multilayer or bulk limit) and  
30  
31 59 monotonically increasing Stark effect coefficient with layer number allows the  
32  
33 60 semiconductor-to-metal transition of few-layer BP to be achieved at a relatively low critical field,  
34  
35 61 for instance, the critical field  $E_c \approx 0.68$  V/nm for 10 layers.<sup>15,16</sup> In addition, according to  
36  
37 62 nonlinear Thomas-Fermi theory, in view of the moderate screening effects of BP, BP flakes  
38  
39 63 thinner than 10-nm will be strongly perturbed by an applied external electrical field.<sup>17</sup> Recently,  
40  
41 64 potassium dopant has been used to tune the electronic bandgap of bulk BP and the transition  
42  
43 65 from a moderate-gap semiconductor to a band-inverted semimetal was induced by applying an  
44  
45 66 ionization-induced vertical electric field.<sup>18</sup> It has also been demonstrated that introducing surface  
46  
47 67 transfer dopants such as caesium carbonate, molybdenum trioxide or depositing cross-linked  
48  
49 68 poly(methyl methacrylate) on BP surface is capable of tuning the transport properties of BP.<sup>19,20</sup>  
50  
51  
52  
53  
54  
55  
56  
57  
58  
59  
60

1  
2  
3  
4 69 However, the drawbacks of chemical doping include instability in air and increased probability  
5  
6 70 of introducing charged scattering centres. In addition, it is difficult to achieve reversible doping  
7  
8 71 using chemical dopants. In contrast, electrostatic doping, which is continuously tunable,  
9  
10 72 non-destructive and carried out in ambient atmosphere, has been widely adopted to tune the  
11  
12 73 optoelectronic properties of 2D materials and their heterostructures.<sup>21-30</sup> It has been predicted  
13  
14 74 from theory that the electrical and optical properties of ultrathin BP can be effectively tuned by  
15  
16 75 electrostatic doping.<sup>15,16,31,32</sup> However, difficulties in the preparation of 2D BP device and its  
17  
18 76 high reactivity when exposed to air have so far limited systematic experimental  
19  
20 77 investigations.<sup>28-30,33-36</sup>  
21  
22  
23  
24

25  
26 78 Here, we report a LT-STM study on a few-layer BP device to demonstrate a giant Stark  
27  
28 79 effect in few-layer BP flakes induced by electrostatic gating. We find that the application of an  
29  
30 80 external perpendicular electric field across few-layer BP flakes leads to a monotonic narrowing  
31  
32 81 of the bandgap with increasing field intensity. We achieve a notable bandgap reduction of  
33  
34 82  $\sim 35.5\%$  (from  $310 \pm 20$  meV to  $200 \pm 20$  meV) by applying a vertical field of 0.1 V/nm. It  
35  
36 83 is expected therefore, that few-layer BP can be transformed from moderate-gap semiconductor to  
37  
38 84 a band-inverted semimetal under a more intense electric field. Furthermore, we observe  
39  
40 85 resonance features in the  $dI/dV$  spectra, which originate from the thickness-dependent sub-band  
41  
42 86 structures in few-layer BP. The gate tunable Stark effect of BP implies that it can be used as an  
43  
44 87 electro-optical modulator operating in the far and mid-infrared regions.  
45  
46  
47  
48  
49

50 88 To probe the effect of the applied electric field on the electronic properties of BP, we  
51  
52 89 prepared a field effect transistor (FET) device consisting of a few-layer-layer BP flake stacked  
53  
54 90 on a SiO<sub>2</sub> substrate with a doped Si back gate as shown in **Figure 1a** (see methods in SI for more  
55  
56 91 details). Using the well-established dry transfer technique, a few-layer BP flake was placed on  
57  
58  
59  
60

1  
2  
3 92 the surface of a pre-patterned gold electrode deposited on a SiO<sub>2</sub>/Si substrate.<sup>37</sup> The gold  
4  
5  
6 93 electrode served as the electrical contact required for STM measurements (Figure 1b). The  
7  
8 94 crystallinity of the BP flake was characterized using Raman spectroscopy. Figure 1c shows the  
9  
10 95 Raman spectrum with the three intrinsic peaks at  $\approx 362.9$ ,  $438.7$ , and  $467.4$  cm<sup>-1</sup>, which are  
11  
12 96 attributed to the A<sub>g</sub><sup>1</sup>, B<sub>2g</sub> and A<sub>g</sub><sup>2</sup> phonon modes respectively, in few-layer BP resulting from its  
13  
14 97 orthorhombic crystal structure (shown in the upper panel of Figure 1b).<sup>7,11,38</sup> To minimize  
15  
16 98 surface degradation, BP devices were immediately loaded into the LT-STM chamber after device  
17  
18 99 fabrication. The thickness of BP flakes probed in our STM study was determined to be  
19  
20  
21  
22 100 equivalent to 11 layers using atomic force microscopy (AFM) (see supporting Figure S1).

23  
24  
25 101 **Figure 2a** shows a typical STM topographic image of a thin BP flake for a scan area of 50  
26  
27 102 nm × 50 nm. It is seen that arrays of one-dimensional (1D) zigzag atomic rows corresponding  
28  
29 103 to the upper rows of atoms in the puckered BP layer are clearly resolved, similar to the atomic  
30  
31 104 STM images of *in-situ* cleaved bulk BP sample in previous reports.<sup>39,40</sup> Our high resolution STM  
32  
33 105 images reveal that an intact BP lattice is present in a majority of the flat surface regions. The  
34  
35 106 defect-related feature showing a bright topographic contrast in STM imaging (Figure 2a), is  
36  
37 107 presumably due to buried impurities or atomic substituents in the BP host lattice. These defects  
38  
39 108 may contribute to hole doping in pristine BP crystals; this aspect is described in a later section.

40  
41  
42 109 According to the atomic structural model of BP (Figure 2b), each P atom is covalently  
43  
44 110 bonded to three nearest neighbour atoms through 3*p* orbitals to form a puckered structure  
45  
46 111 consisting of an upper row of P atoms (red and white balls) and a lower row of P atoms (violet  
47  
48 112 balls). The wave function of the lower P atoms is expected to decay exponentially in the vertical  
49  
50 113 direction and thus only the P atoms located on the top are clearly resolved in the STM  
51  
52 114 topographic image as shown in the close up image (Figure 2c). The lattice constants measured

1  
2  
3  
4 115 along two directions (armchair “xx” and zigzag “xy” shown in Figure 2b, top view) are  
5  
6 116 determined to be  $4.46 \pm 0.13 \text{ \AA}$  and  $3.32 \pm 0.05 \text{ \AA}$ , respectively, which are in good agreement  
7  
8 117 with previously reported values for bulk BP.<sup>12,13,39,40</sup> Figure 2d shows a wide energy range  $dI/dV$   
9  
10 118 spectrum (which reflects the local density of states, LDOS) collected from areas on the BP  
11  
12 119 surface far away from defective regions. The intrinsic spectrum is highly asymmetric and shows  
13  
14 120 a wide “gap-like” signature surrounded by a series of well-defined resonant peaks labelled as  $V_n$   
15  
16 121 in the valence band and  $C_m$  in the conduction band. The origin of these prominent resonance  
17  
18 122 features will be discussed later in the article. Due to the relatively large tip-sample separation,  
19  
20 123 the  $dI/dV$  signal in the vicinity of the Fermi energy ( $E_F$ ,  $V_S = 0 \text{ V}$ ) is low and thus the prominent  
21  
22 124 features in the spectrum occurs at high energy away from  $E_F$ .<sup>21,39-41</sup> To better resolve the  
23  
24 125 electronic states close to  $E_F$ , a lower set point ( $V_S = -1.0 \text{ V}$ ,  $I = 1.0 \text{ nA}$ ) has been used to collect  
25  
26 126 the  $dI/dV$  spectrum from the same surface region as shown in Figure 2f. The bandgap of the  
27  
28 127 as-prepared BP ( $E_g = E_{\text{CBM}} - E_{\text{VBM}}$ , see supporting Figure S2 for details of the calculation) is  
29  
30 128 determined to be  $310 \pm 20 \text{ meV}$ , consistent with previously reported behaviour and values for  
31  
32 129 bulk BP.<sup>12,40</sup> The slight fluctuation of  $E_g$  may be attributed to a tip-induced band bending effect,  
33  
34 130 which has been carefully investigated in this work (see supporting information for details). Our  
35  
36 131 STS data also reveal that the as-prepared BP flakes are heavily p-doped, which is confirmed  
37  
38 132 from the closeness of the VBM energy and  $E_F$  (Figure 2f).  
39  
40  
41  
42  
43  
44  
45  
46

47 133 Next, we probe the evolution of the local electronic properties of BP as a function of the  
48  
49 134 applied back gate voltage ( $V_g$ ). In contrast to n-doping using K atoms, electrostatic gating  
50  
51 135 enables us to tune the doping levels in thin BP flakes to obtain p-type or n-type behavior.<sup>18</sup>  
52  
53 136 **Figure 3a** shows the gate-voltage-dependent STS spectra acquired in the defect-free region of  
54  
55 137 the 11-layer BP flake. At positive gate voltages ( $V_g > 0 \text{ V}$ ), negative charge carriers are injected  
56  
57  
58  
59  
60

1  
2  
3  
4 138 into the BP flake leading to n-type doping of BP. Hence, the band structure shifts towards the  
5  
6 139 negative sample bias region [from the green line (0 V) up to the red line (+60 V)]. To our  
7  
8 140 surprise, the shift of the band structure towards higher potential energy [(from the green line (0 V)  
9  
10  
11 141 down to the blue line (−60 V)] is negligible. This observation is tentatively attributed to the  
12  
13 142 heavily p-doped nature of the thin BP flakes ( $E_F$  is located at the edge of the VB and the presence  
14  
15 143 of shallow acceptor states), which leads to Fermi level pinning. In order to determine the values  
16  
17  
18 144 of the VBM, CBM and bandgap more accurately, the logarithm of the  $dI/dV$  spectra collected at  
19  
20 145 different gate voltages on thin BP flakes were plotted (shown in Figure 3b and 3c) (refer to  
21  
22 146 supporting Figure S2 for more details). Using this method, we extracted the gate-dependent  
23  
24  
25 147 energies corresponding to CBMs, VBMs and the resonance peaks as shown in Figure 3d. It can  
26  
27 148 be clearly observed that the CBMs and VBMs (pinned at the  $E_F$ ) barely shift at  $V_g \leq 0$  V, and  
28  
29  
30 149 consequently, the overall shift in the band structure of BP is negligible. In contrast, at  $V_g \geq 0$  V,  
31  
32 150 a pronounced downward shift of the entire band structure is observed. Interestingly, we also  
33  
34 151 observed that the bandgap reduces significantly with increase in applied gate voltages at  $V_g \geq 0$   
35  
36  
37 152 V. In addition, the observed resonance peaks at different gate voltages move with the band edges  
38  
39 153 depending on whether they are in the conduction band or the valence band region.

40  
41  
42 154 Here we employ Scanning Tunnelling Spectroscopy (STS) to measure field-dependent  
43  
44 155 single-particle electronic bandgap of few-layer BP as opposed to two-particle optical bandgap  
45  
46  
47 156 *via* optical adsorption.<sup>41</sup> Hence, the reduction in the bandgap of 11-layer BP flakes as a function  
48  
49  
50 157 of gate voltages can be explained on the basis of a giant Stark effect rather than Franz-Keldysh  
51  
52 158 effect reported in the recent work on optoelectronic modulation of BP.<sup>28,29,42</sup> In the absence of a  
53  
54 159 giant Stark effect, a rigid band shift typically occurs with gate voltage and  $E_g$  remains unchanged  
55  
56  
57 160 even when electric field is applied (**Figure 4a**, left.  $E_g = E'_g = \text{constant}$ ).<sup>24,43</sup> In the presence of



1  
2  
3  
4 161 the Stark effect, the band edges of VB and CB gradually move towards each other with  
5  
6 162 increasing gate voltage due to the spatial redistribution of their wave functions in the puckered  
7  
8 163 layer structure, as shown in Figure 4a (right). To understand the asymmetry in gap reduction  
9  
10 164 observed in Figure 3a and 3d, we provide a schematic to explain the experimental results at  
11  
12 165 different gate bias. Initially ( $V_g = 0$  V, left panel of Figure 3e), the few-layer BP sample is  
13  
14 166 p-doped (VBM of BP flake nearly touches the Fermi energy, Figure 2f and green line in Figure  
15  
16 167 3b) and therefore, free positive charge carriers distribute uniformly in the real space of few-layer  
17  
18 168 BP. When a negative gate voltage is applied ( $V_g < 0$  V, electrons accumulate in the p++ silicon  
19  
20 169 layer and thus holes will be induced in the BP layers), additional holes fill the valence states. As  
21  
22 170 a result of the accumulation of holes, screening of the gate electric field occurs (right panel in  
23  
24 171 Figure 3e) and the measured bandgap of BP remains approximately constant (Figure 3b). On the  
25  
26 172 other hand, a positive gate voltage injects electrons into the BP flake. A depletion layer is formed  
27  
28 173 with different heights depending on the field strength (left panel, Figure 3f), which facilitates the  
29  
30 174 penetration of the electric field into the whole BP flake (right panel, Figure 3e). During this  
31  
32 175 process, two effects can occur: i) a potential drop that shifts the CB and the VB towards lower  
33  
34 176 energy and ii) a gap reduction due to the Stark effect as shown in Figure 3c ( $V_g = 0$  V, 20V and  
35  
36 177 30V). With increasing voltage ( $E_F$  locates right in the middle of bandgap, here,  $V = 29 \pm 1$  V),  
37  
38 178 the holes become completely depleted by back-gating. At even higher positive gate voltages, the  
39  
40 179 BP flake becomes electron doped, (as shown in Figure 3f, right panel) and both the VB and the  
41  
42 180 CB move towards the negative sample bias region with the latter approaching the Fermi level.  
43  
44 181 Once the CB touches the Fermi level, the “pinning” effect dominates and the gap reduction is  
45  
46 182 arrested. For the latter two cases shown in Figure 3f ( $V_g > 0$  V), the bandgap of few-layer BP is  
47  
48 183 reduced to  $200 \pm 20$  meV even at a moderate gate voltage ( $V_g = 60$  V), due to the giant Stark  
49  
50  
51  
52  
53  
54  
55  
56  
57  
58  
59  
60

184 effect.<sup>1,2,16</sup> The magnitude of bandgap modulation achievable by the Stark effect is predicted to  
 185 be larger in thinner BP flakes due to its larger bandgap as compared to thicker BP, where  
 186 electro-optical modulation from the visible to far infrared regime can be achieved in monolayer  
 187 and bilayer BP.<sup>7,15,16</sup> Our theoretical calculations reveal that the Stark coefficient defined as  $S_{nL} =$   
 188  $-(dE_g/dE_{ext})/e$  increases monotonically as a function of layer thickness (see supporting Figure  
 189 S3), suggesting that a large critical field strength is required to induce the  
 190 semiconductor-to-semimetal phase transition for thinner samples.

191 In order to estimate the magnitude of reduction of  $E_g$  by Stark effect and to identify the  
 192 origin of the resonance peaks in the  $dI/dV$  spectra, we calculate the electronic structure of  
 193 few-layer BP under different external electrical fields, using density functional theory (DFT)  
 194 calculations within the Perdew-Burke-Ernzerhof parametrisation (PBE).<sup>12,16</sup> Figure 4b shows the  
 195 highest occupied states at the  $\Gamma$  point for a 11-layer BP sample without (top) and with (bottom)  
 196 0.1 V/nm electrical field, where a strong redistribution of the VBM states along the  $z$  direction is  
 197 observed in the latter. Even though the value of the estimated bandgap is slightly underestimated  
 198 using the PBE approximation, modifications of the band structure due to small perturbations can  
 199 be correctly predicted. For low fields, it is found that the bandgap varies quadratically with the  
 200 electric field as expected from the system symmetry. Since phosphorene is centrosymmetric and  
 201 has no dipole in the direction of the field, the first order term in the expression for the energy  
 202 levels  $\varepsilon_i$  in  $E$  vanishes, and the leading terms are (as found by perturbation theory) given by :

$$203 \quad \varepsilon_i = \varepsilon_i^0 + \sum_{k \neq i} \frac{M_{ik}^{zz}}{\varepsilon_i - \varepsilon_k} E^2 \quad (1)$$

204 where  $M_{ik}^{zz}$  is the dipole matrix element between states  $i$  and  $k$ .

1  
2  
3  
4 205 This is qualitatively similar to the experimentally observed behaviour (Figure 4c). If the intensity  
5  
6 206 of the electric field is calculated from the experimental values for  $V_g$  assuming that the system  
7  
8 207 can be approximated by two planar capacitors in series (see supporting Figure S4 for more  
9  
10 208 details), the experimentally obtained rate  $dE_g/dE$  is of the same order of magnitude as  
11  
12 209 expected from the theoretical prediction (inset in Figure 4c), despite despite the bandgap  
13  
14 210 underestimation, the uncertainty in the estimation of the capacitance, and tip-induced band  
15  
16 211 bending effects which may contribute to decrease the measured  $dE_g/dE$ .<sup>24,44,45</sup> In fact, a large  
17  
18 212 magnitude of bandgap reduction should be achievable by applying a high electric field. By  
19  
20 213 performing transport studies on a dual-gated BP transistor, Deng *et al.* reported that the band gap  
21  
22 214 can be narrowed to  $\sim 50$  meV under a high electric field strength of 1.1 V/nm by measuring the  
23  
24 215 minimum transport conductivity and carrier density at different temperatures.<sup>30</sup>

25  
26  
27  
28  
29  
30 216 In the STS spectra (Figure 2d and 2f) of the 11-layer BP flake, in addition to the gap feature,  
31  
32 217 resonance peaks are observed. The tendency of these peaks to move in the same direction as the  
33  
34 218 band edges as a function of the gate voltage indicates that they originate from electronic states  
35  
36 219 and are not due to tip-induced charging effects (see supporting Figure S5).<sup>22,41</sup> The energy  
37  
38 220 separation between the adjacent resonances observed here is larger than 150 meV, which is much  
39  
40 221 higher than the energy of the most energetic phonon mode of BP ( $\sim 66.1$  meV).<sup>38</sup> The  
41  
42 222 nearly-rigid shifting of the resonance peaks together with the band edges also rules out possible  
43  
44 223 contribution from electron-plasmon coupling (see supporting information for more details on  
45  
46 224 other possible origins of these peaks).<sup>46-48</sup> Instead, a sub-band model due to the quantisation of  
47  
48 225 BP layers with finite thickness can be used to explain the thickness-dependent resonance features  
49  
50 226 in the STS spectra, which is verified both by our DFT calculations with PBE and through a  
51  
52 227 phenomenological tight-binding model.<sup>14,49</sup> LDOS obtained from DFT calculations are in good

228 agreement with the STS spectra recorded on BP with different layer numbers (see supporting  
229 Figure S6). Due to the strong interlayer interaction, both the CBs and VBs of N-layer  
230 phosphorene are quantized and split into N 2D sub-bands. This quantum-well like structure  
231 creates the characteristic sub-band structures of few-layer BP, which in turn modifies its density  
232 of states. In the absence of other interactions and thermal effects, this DOS modulation may  
233 manifest as singularities in a system with a parabolic band dispersion. The spacing between the  
234 peaks can be approximated by a simple one dimensional tight-binding band model

$$E_{N,n} = E_{N,n}^0 + 2\gamma \cos\left(\frac{n\pi}{N+n}\right) \quad (2)$$

236 where  $n = 1, 2, \dots, N$ , is the subband index,  $E_{N,n}^0$  is the average band energy, and  $\gamma = 0.55$   
237 (HSE), 0.49 (PBE). Based on this simplified tight-binding model, an integrated evolution of the  
238 sub-band structures of few-layer BP is empirically described (Figure 4d). This model describes  
239 the band energy at the  $\Gamma$  point of the 2D Brillouin zone considering only the nearest-neighbour  
240 layer-layer interaction while neglecting electron-electron and electron-hole (exciton effect)  
241 interactions, in accordance with our experimental conditions.

242 To further elucidate the nature of the resonance peaks in STS, we compare the experimental  
243  $dI/dV$  spectra with the DOS obtained from DFT calculations for few-layer BP ranging from 1–12  
244 layers (Figure 4e, see supporting Figure S7 for a full version). The large hole effective mass  
245 along the  $\Gamma - Y$  direction leads to additional contributions in DOS, which gives rise to the  
246 observed peaks in STS (shown in Figure 2f). Moreover, the sharp peaks which are seen  
247 appearing in the -1.5 to -2 eV energy range ( $V'_n$ , Figure 2d) originate from deep-lying flat  
248 sub-bands. Our calculations confirm the presence of sub-bands with energy spacing similar to the  
249 experimentally observed resonance peaks. One remarkable feature is the possibility for optical

1  
2  
3 250 transitions between quantized sub-bands in the same band, leading to multiphoton absorptions.  
4  
5  
6 251 The unique sub-band structure also suggests that BP may qualify as an emerging candidate  
7  
8 252 material for quantum cascade lasers.<sup>50</sup>  
9  
10

11 253 The giant Stark effect in few-layer BP device allows the bandgap of BP to be electrically  
12  
13 254 tuned. For 11-layer-thick BP, the bandgap can be reduced from  $310 \pm 20$  meV to  $200 \pm 20$   
14  
15 255 meV. Interestingly, layer-dependent sub-band structures (especially the sub-bands at  $\Gamma$  point)  
16  
17 256 have been experimentally observed in our STS measurements, where we found that the number  
18  
19 257 of sub-bands is directly correlated to the number of layers in BP. This suggests that STS can be  
20  
21 258 used as a tool to accurately determine the layer number in few-layer BP. The reduced bandgap of  
22  
23 259 few-layer BP due to the giant Stark effect shifts its working spectral range to far-IR while the  
24  
25 260 sub-band transition induces multiphoton absorptions.<sup>50-52</sup> Moreover, the giant Stark effect breaks  
26  
27 261 the symmetric BP quantum well-like electronic structure, leading to the relaxation of selection  
28  
29 262 rules and consequently activates “forbidden” optical transitions from the valence sub-band to the  
30  
31 263 conduction sub-band with different quantum numbers.<sup>52</sup> Our work suggests that the inter-band  
32  
33 264 and inter sub-band transitions in BP can be continuously varied over a wide electromagnetic  
34  
35 265 spectral range from visible to far IR by varying the electric field, making BP a versatile material  
36  
37 266 platform for applications in IR optical modulators and quantum cascade lasers.  
38  
39  
40  
41  
42  
43  
44  
45  
46  
47

## 48 **ASSOCIATED CONTENT**

49  
50  
51 269 The Supporting Information is available free of charge on the ACS Publications website.  
52

53 270 Details of the experiment method, thickness determination, bandgap calculation method,  
54  
55 271 layer-dependent properties of BP, exclusion of possible origin of resonance peaks, calculated  
56  
57 272 band structure of 1-12 layer BP.  
58  
59  
60

1  
2  
3 273 **AUTHOR INFORMATION**  
4

5  
6 274 **Corresponding Authors:**  
7

8  
9 275 \*K. P. L. (E-mail: chmlohkp@nus.edu.sg)  
10

11 276 \*J. L. (E-mail: chmluj@nus.edu.sg)  
12  
13

14 277 **ORCID**  
15

16  
17 278 Yanpeng LIU: 0000-0002-5265-2735  
18

19  
20 279 Sherman J. R. Tan: 0000-0003-1591-3497  
21

22 280 Kian Ping Loh: 0000-0002-1491-743X  
23

24  
25 281 Jiong Lu: 0000-0002-3690-8235  
26

27  
28 282 **Author contributions**  
29

30  
31 283 ¶These authors contribute equally to this work.  
32

33  
34 284 **Notes**  
35

36  
37 285 The authors declare no competing financial interests.  
38

39 286 **ACKNOWLEDGMENTS**  
40

41  
42 287 The authors acknowledge the National Research Foundation, Prime Minister Office, Singapore,  
43  
44 288 under its Medium Sized Centre Programme and CRP award “Novel 2D materials with tailored  
45  
46 289 properties: Beyond graphene” (R-144-000-295-281). The first-principles calculations were  
47  
48 290 carried out on the Centre for Advanced 2D Materials computing facilities. J. Lu acknowledges  
49  
50 291 the support from NUS start-up grant (R-143-000-621-133) and Tier 1 (R-143-000-637-112).  
51  
52  
53  
54

55 292

56 293  
57  
58  
59  
60

## 294 REFERENCES

- 295 1. Park, C.-H.; Louie, S. G. *Nano Lett.* **2008**, *8*, 2200-2203.
- 296 2. Khoo, K. H.; Louie, S. G. *Phys. Rev. B*, **2004**, *69*, 201401.
- 297 3. Kuo, Y.; Lee, Y. K.; Ge, Y.; Ren, S.; Roth, J. E.; Kamins, T. I.; Miller, D. A. B.; Harris, J. S.  
298 *Nature*, **2005**, *437*, 1334-1336.
- 299 4. Fröhlich, D.; Wille, R.; Schlapp, W.; Weimann, G. *Phys. Rev. Lett.* **1987**, *59*, 1748.
- 300 5. Ramasubramaniam, A.; Naveh, D.; Towe, E. *Phys. Rev. B*, **2011**, *84*, 205325.
- 301 6. Li, L.; Yu, Y.; Ye, G. J.; Ge, Q.; Ou, X.; Wu, H.; Feng, D.; Chen, X. H.; Zhang, Y. *Nat.*  
302 *Nanotech.*, **2014**, *9*, 372-377.
- 303 7. Ling, X.; Wang, H.; Huang, S.; Xia, F.; Dresselhaus, M. S. *Proc. Natl Acad. Sci. USA*. **2015**,  
304 *112*, 4523-4530.
- 305 8. Churchill, H. O.; Jarillo-Herrero, P. *Nat. Nanotech.* **2014**, *9*, 330-331.
- 306 9. Liu, H.; Du, Y.; Deng, Y.; Peide, D. Y. *Chem. Soci. Rev.* **2015**, *44*, 2732-2743.
- 307 10. Reich, E. S. *Nature*. **2014**, *506*, 19.
- 308 11. Castellanos-Gomez, A. *J. Phys. Chem. Lett.* **2015**, *6*, 4280-4291.
- 309 12. Qiao, J.; Kong, X.; Hu, Z. X.; Yang, F.; Ji, W. *Nat. Commun.* **2014**, *5*.
- 310 13. Low, T.; Rodin, A. S.; Carvalho, A.; Jiang, Y.; Wang, H.; Xia, F.; Neto, A. C. *Phys. Rev. B*.  
311 **2014**, *90*, 075434.
- 312 14. Li, L.; Kim, J.; Jin, C.; Ye, G.; Qiu, D. Y.; da Jornada, F. H.; Shi, Z.; Chen, L.; Zhang, Z.;  
313 Yang, F.; Watanabe, K.;. *Nat. Nanotech.* **2016**, *12*, 21-25.
- 314 15. Li, Y.; Yang, S.; Li, J. *J. Phys. Chem. C*, **2014**, *118*, 23970-23976.
- 315 16. Dolui, K.; Quek, S. Y. *Sci. Rep.* **2015**, *5*, 11699.
- 316 17. Low, T.; Roldán, R.; Wang, H.; Xia, F.; Avouris, P.; Moreno, LM.; Guinea, F. *Phys. Rev.*  
317 *Lett.* **2014**, *113*, 106802.
- 318 18. Kim, J.; Baik, S.S.; Ryu, S.H.; Sohn, Y.; Park, S.; Park, B.G.; Denlinger, J.; Yi, Y.; Choi,  
319 H.J.; Kim, K.S. *Science*. **2015**, *349*, 723-726.
- 320 19. Wang, G.; Bao, L.; Pei, T.; Ma, R.; Zhang, Y. Y.; Sun, L.; Zhang, G.; Yang, H.; Li, J.; Gu,  
321 C.; Du, S.; *Nano Lett.* **2016**, *16*, 6870.
- 322 20. Xiang, D.; Han, C.; Wu, J.; Zhong, S.; Liu, Y.; Lin, J.; Zhang, X.-A.; Ping, H. W.;  
323 Özyilmaz, B.; Neto, A. H. C. *Nat. Commun.* **2015**, *6*, 6485.

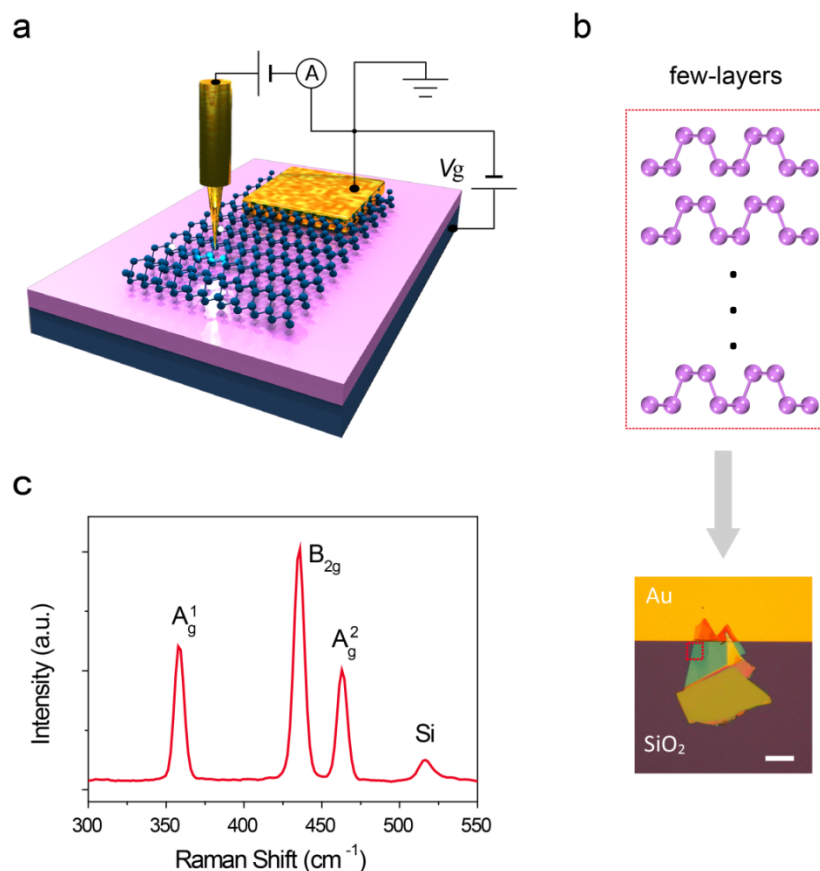
- 1  
2  
3  
4 324 21. Zhang, Y.; Brar, V.W.; Wang, F.; Girit, C.; Yayon, Y.; Panlasigui, M.; Zettl, A.; Crommie,  
5 325 M.F. *Nat. Phys.* **2008**, *4*, 627-630.
- 6  
7 326 22. Zhang, Y.; Tang, T.T.; Girit, C.; Hao, Z.; Martin, M.C.; Zettl, A.; Crommie, M.F.; Shen,  
8 327 Y.R.; Wang, F. *Nature*. **2009**, *459*, 820-823.
- 9  
10 328 23. Khodkov, T.; Khrapach, I.; Craciun, M. F.; Russo, S. *Nano Lett.* **2015**, *15*, 4429-4433.
- 11  
12 329 24. Lu, C. P.; Li, G.; Mao, J.; Wang, L. M.; Andrei, E. Y. *Nano Lett.* **2014**, *14*, 4628-4633.
- 13  
14 330 25. Chu, T.; Ilatikhameneh, H.; Klimeck, G.; Rahman, R.; Chen, Z. *Nano Lett.* **2015**, *15*,  
15 331 8000-8007.
- 16  
17 332 26. Xue, J.; Sanchez-Yamagishi, J.; Bulmash, D.; Jacquod, P.; Deshpande, A.; Watanabe, K.;  
18 333 Taniguchi, T.; Jarillo-Herrero, P.; LeRoy, B.J. *Nat. Mater.* **2011**, *10*, 282-285.
- 19  
20 334 27. Yankowitz, M.; Xue, J.; Cormode, D.; Sanchez-Yamagishi, J.D.; Watanabe, K.; Taniguchi,  
21 335 T.; Jarillo-Herrero, P.; Jacquod, P.; LeRoy, B.J. *Nat. Phys.* **2012**, *8*, 382-386.
- 22  
23 336 28. Lin, C.; Grassi, R.; Low, T.; Helmy, A.S. *Nano Lett.* **2016**, *16*, 1683-1689.
- 24  
25 337 29. Whitney, W.S.; Sherrott, M.C.; Jariwala, D.; Lin, W.H.; Bechtel, H.A.; Rossman, G.R.;  
26 338 Atwater, H.A. *Nano Lett.*, **2017**, *17*, 78-84.
- 27  
28 339 30. Deng, B.; Tran, V.; Jiang, H.; Li, C.; Xie, Y.; Guo, Q.; Wang, X.; Tian, H.; Wang, H.; Cha,  
29 340 J.J.; Xia, Q. arXiv preprint arXiv:1612.04475. **2016**, 1612.
- 30  
31 341 31. Yuan, S.; van Veen, E.; Katsnelson, M.I.; Roldán, R. *Phys. Rev. B* **2016**, *93*, 245433.
- 32  
33 342 32. Liu, Q.; Zhang, X.; Abdalla, L. B.; Fazio, A.; Zunger, A. *Nano Lett.* **2015**, *15*, 1222-1228.
- 34  
35 343 33. Wood, J.D.; Wells, S.A.; Jariwala, D.; Chen, K.S.; Cho, E.; Sangwan, V.K.; Liu, X.; Lauhon,  
36 344 L.J.; Marks, T.J.; Hersam, M.C. *Nano Lett.* **2014**, *14*, 6964-6970.
- 37  
38 345 34. Castellanos-Gomez, A.; Vicarelli, L.; Prada, E.; Island, J. O.; Narasimha-Archarya, K. L.;  
39 346 Blanter, S. I.; Groenendijk, D. J.; Buscema, M.; Steele, G. A.; Alvarez, J. V.; Zandbergen, H.  
40 347 W.; Palacios, J. J.; van der Zant, H. S. J. *2D Mater.* **2014**, *1*, 025001.
- 41  
42 348 35. Favron, A.; Gaufres, E.; Fossard, F.; Phaneuf-L'Heureux, A.L.; Tang, N.Y.; Lévesque, P.L.;  
43 349 Loiseau, A.; Leonelli, R.; Francoeur, S.; Martel, R. *Nat. Mater.* **2015**, *14*, 826-832.
- 44  
45 350 36. Kim, J.-S.; Liu, Y.; Zhu, W.; Kim, S.; Wu, D.; Tao, L.; Dodabalapur, A.; Lai, K.;  
46 351 Akinwande, D. *Sci. Rep.* **2015**, *5*, 8989.
- 47  
48 352 37. Castellanos-Gomez, A.; Buscema, M.; Molenaar, R.; Singh, V.; Janssen, L.; van der Zant,  
49 353 H.S.; Steele, G.A. *2D Mater.* **2014**, *1*, 011002.
- 50  
51 354 38. Aierken, Y.; Çakır, D.; Sevik, C.; Peeters, F. M. *Phys. Rev. B* **2015**, *92*, 081408.
- 52  
53  
54  
55  
56  
57  
58  
59  
60



- 1  
2  
3  
4 355 39. Liang, L.; Wang, J.; Lin, W.; Sumpter, B. G.; Meunier, V.; Pan, M. *Nano Lett.* **2014**, *14*,  
5 356 6400-6406.
- 6  
7 357 40. Zhang, C.D.; Lian, J.C.; Yi, W.; Jiang, Y.H.; Liu, L.W.; Hu, H.; Xiao, W.D.; Du, S.X.; Sun,  
8 358 L.L.; Gao, H.J. *J. Phys. Chem. C.* **2009**, *113*, 18823-18826.
- 9  
10 359 41. Ugeda, M.M.; Bradley, A.J.; Shi, S.F.; Felipe, H.; Zhang, Y.; Qiu, D.Y.; Ruan, W.; Mo, S.K.;  
11 360 Hussain, Z.; Shen, Z.X.; Wang, F.; *Nat. Mater.*, **2014**, *13*, 1091-1095.
- 12  
13 361 42. Miller, D.A.B.; Chemla, D.S.; Schmitt-Rink, S. *Phys. Rev. B*, **1986**, *33*, 6976.
- 14  
15 362 43. Klein, J.; Wierzbowski, J.; Regler, A.; Becker, J.; Heimbach, F.; Müller, K.; Kaniber, M.;  
16 363 Finley, J.J. *Nano Lett.* **2016**, *16*, 1554-1559.
- 17  
18 364 44. Brar, V.W.; Decker, R.; Solowan, H.M.; Wang, Y.; Maserati, L.; Chan, K.T.; Lee, H.; Girit,  
19 365 Ç.O.; Zettl, A.; Louie, S.G.; Cohen, M.L.; *Nat. Phys.* **2011**, *7*, 43-47.
- 20  
21 366 45. Luryi, S. *Appl. Phys. Lett.* **1988**, *52*, 501-503.
- 22  
23 367 46. Bostwick, A.; Ohta, T.; Seyller, T.; Horn, K.; Rotenberg, E. *Nat. Phys.* **2007**, *3*, 36-40.
- 24  
25 368 47. Brar, V.W.; Wickenburg, S.; Panlasigui, M.; Park, C.H.; Wehling, T.O.; Zhang, Y.; Decker,  
26 369 R.; Girit, Ç.; Balatsky, A.V.; Louie, S.G.; Zettl, A.; *Phys. Rev. Lett.* **2010**, *104*, 036805.
- 27  
28 370 48. Girard, J. C.; Lemaître, A.; Miard, A.; David, C.; Wang, Z. Z. *J. Vac. Sci. Technol. B.* **2009**,  
29 371 *27*, 891-894.
- 30  
31 372 49. Zhang, G.; Chaves, A.; Huang, S.; Song, C.; Low, T.; Yan, H. *arXiv preprint*  
32 373 *arXiv:1607.08049*. **2016**, 1607.
- 33  
34 374 50. Sirtori, C.; Faist, J.; Capasso, F.; Cho, A. Y. *Pure. Appl. Opt.: J. Euro. Opti. Soc. Part A.*  
35 375 **1998**, *7*, 373.
- 36  
37 376 51. Rogalski, A. *Infrared phys. & technol.* **2007**, *50*, 240-252.
- 38  
39 377 52. Sun, Z.; Martinez, A.; Wang, F. *Nat. Photon.*, **2016**, *10*, 227-238.
- 40  
41  
42  
43  
44 378

379 **Figures and Legends**

380

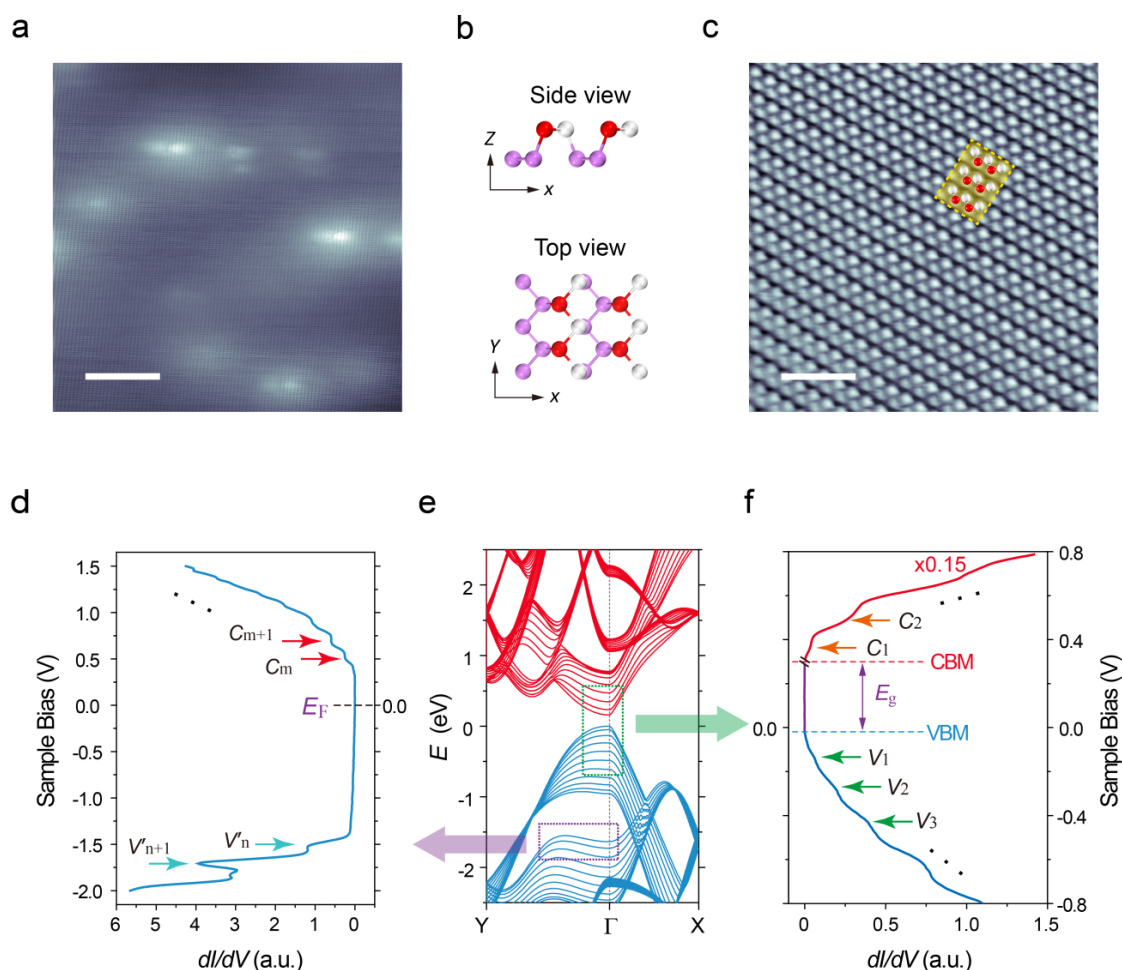


381

382 **Figure 1.** Schematic drawing and structural characterisation of a few-layer BP device. (a) Schematic  
383 illustration of a gated BP device during STM analysis. The sample bias  $V_s$  is applied between the STM tip  
384 and the thin BP sample contacted by a gold electrode. The electrostatic gate voltage is applied to the BP  
385 flake through a p-doped silicon wafer. (b) Optical image of few-layer BP flakes on silicon substrate  
386 partially in contact with a gold electrode. Scale bar is 20  $\mu\text{m}$ . (c) Raman spectrum of the as-prepared BP  
387 flake; the peak at  $\sim 520 \text{ cm}^{-1}$  originates from the underlying silicon substrate.

388

389

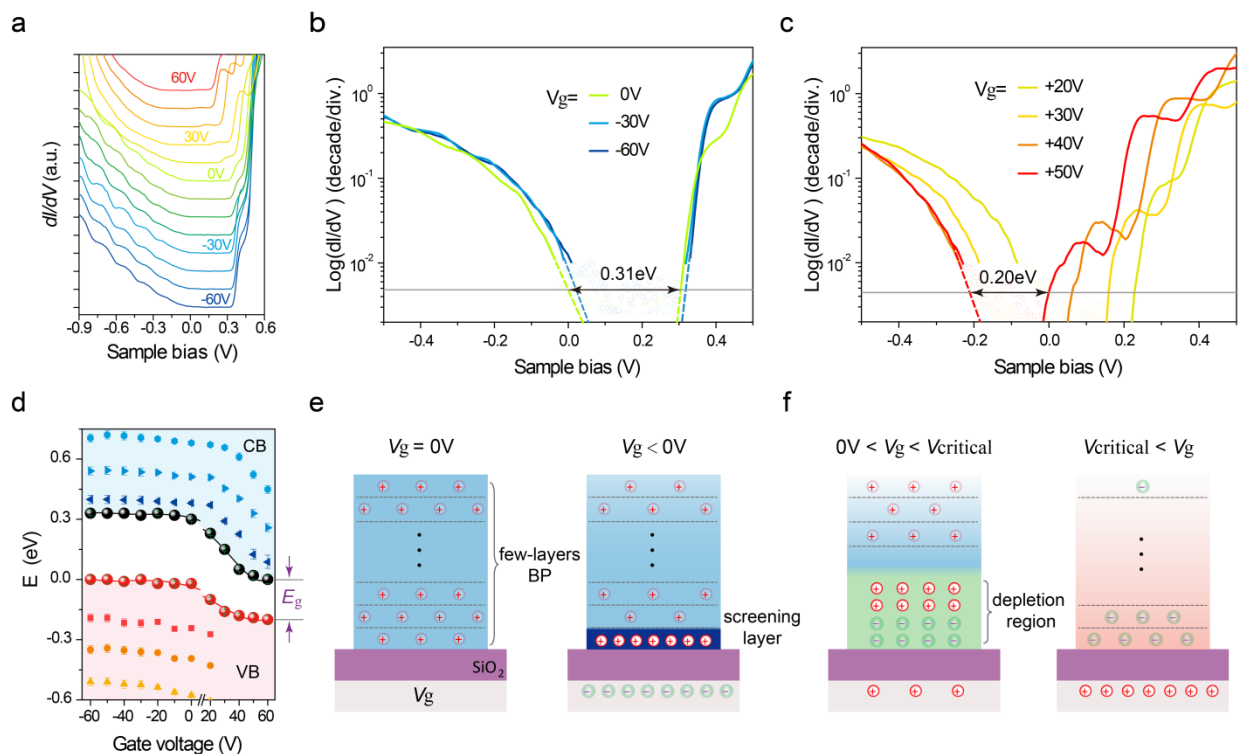


390

391 **Figure 2.** STM imaging and electronic characterization of a few-layer BP device. (a) Large-area STM  
 392 imaging of the bare BP flake ( $V_S = -0.3$  V,  $I = 0.6$  nA). Scale bar is 10 nm. (b) Sketches showing the side  
 393 and top view of monolayer BP. Scale bar is 10 nm. (c) High-resolution STM image of BP ( $V_S = -0.35$  V,  
 394  $I = 0.8$  nA). Scale bar is 1.5 nm. (d) A wide energy range  $dI/dV$  spectrum acquired on few-layer BP  
 395 showing the electronic resonance features  $V'_n$  in the valence band and  $C_m$  in the conduction band.  $E_F$   
 396 represents Fermi energy (set point:  $V_S = -2.0$  V,  $I = 2.5$  nA). (e) PBE band structure calculation of  
 397 11-layer BP. (f) a narrow energy range  $dI/dV$  spectrum taken on the same spot (as that in d) revealing the  
 398 valence band maximum, the conduction band minimum and a few resonance peaks ( $V_n$  in VB region and  
 399  $C_m$  in CB region). CB region (red line) is rescaled by a factor of 0.15 for visual contrast.

400

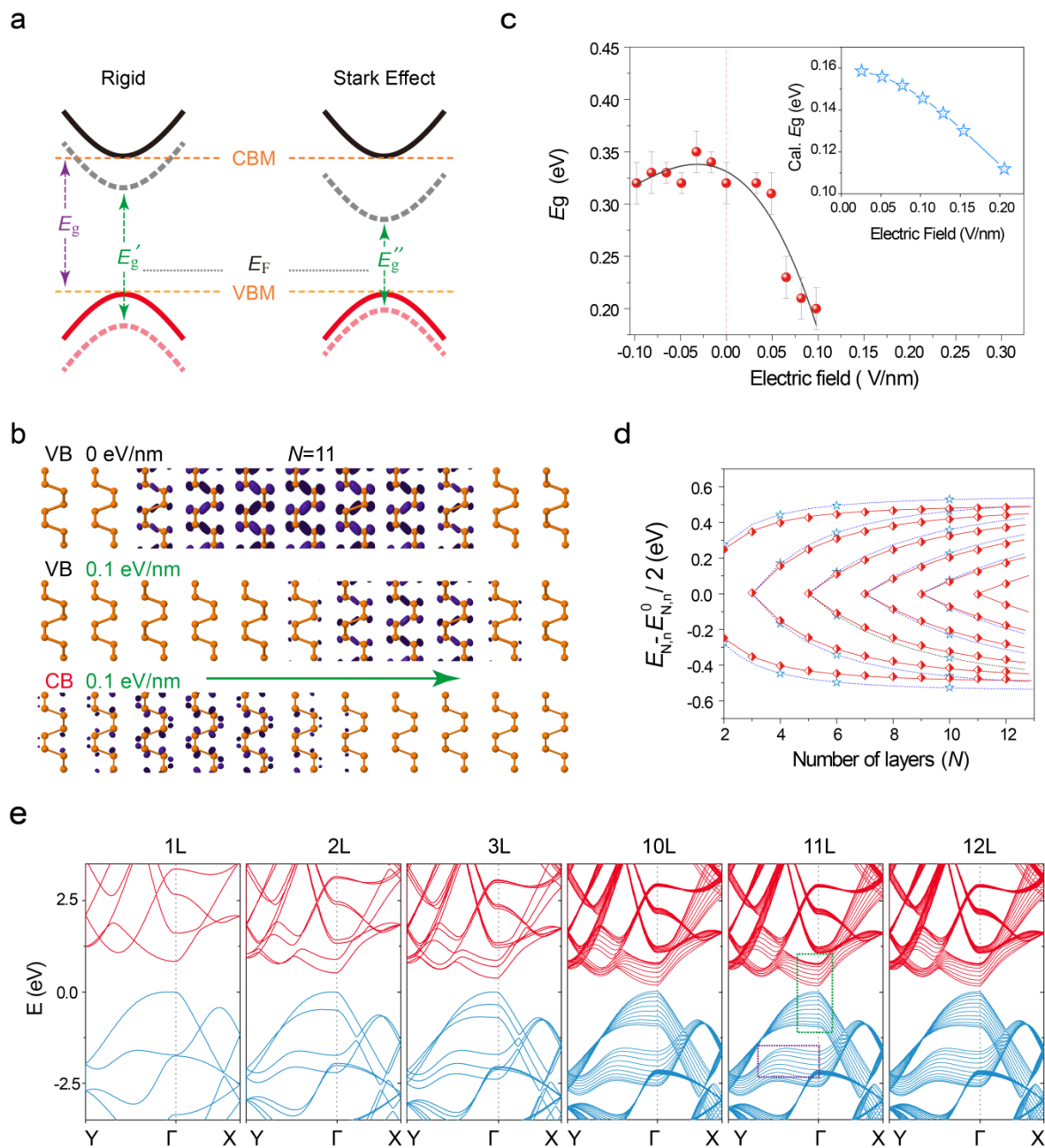
401



402

403 **Figure 3.** Gate-controlled Stark effect in an 11-layer BP flake device. (a) Gate-dependent  $dI/dV$  spectra  
 404 obtained on a defect free region in an 11-layer BP flake. (Set point:  $V_S = -1.0$  V,  $I = 1.0$  nA). The curves  
 405 are vertically offset and the gate voltage step is 10 V. (b) and (c) Logarithmic  $dI/dV$  spectra under  
 406 negative and positive gate voltages, respectively. (d) VBM (red balls), CBM (black balls), resonance  
 407 peaks (solid symbols) and bandgap ( $E_g$ ) of 11-layer BP at different gate voltages. (e) and (f) Schematic  
 408 models (note: thickness and charge carrier density not to scale) to illustrate the charge carrier distribution  
 409 and gate-dependent behaviour of 11-layer BP shown in Figure 3b and 3c, respectively.

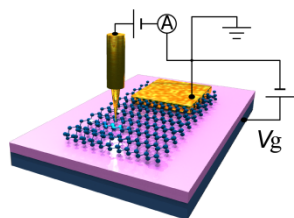
410



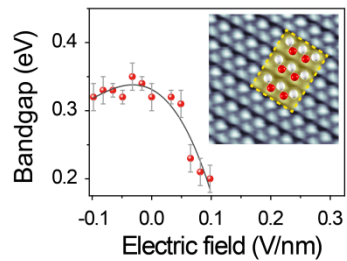
**Figure 4.** Calculated electronic structures of few-layer BP with and without field modulation. (a) Schematic illustration of the field modulation of electronic structures of few-layer BP with and without a giant Stark effect. The solid red and black lines indicate the initial positions of VBM and CBM ( $E=0$  V) while the dashed red and black lines represent the VBM and CBM under an electric field ( $E \neq 0$  V), respectively. (b) The wave function modulus square of the highest occupied state at  $\Gamma$  point for 11-layer BP sample at 0 V/nm (top) and 0.1 V/nm (middle) electrical fields. The wave function modulus square of the lowest unoccupied state at  $\Gamma$  point for the 11-layer BP sample at 0.1 V/nm electrical field (bottom). (c)

1  
2  
3 419 Measured bandgap of 11-layer BP as a function of applied electrical field. Inset shows the calculated  
4  
5 420 bandgap of a BP sample of the same thickness in the presence of electrical fields of different strength. (d)  
6  
7 421 Level spacing in few-layer BP (layer number  $N= 2-12$ ) obtained from PBE (red) and HSE (blue)  
8  
9 422 calculation methods. (e) Representative layer-dependent PBE band structures of BP; please refer to the  
10 423 supporting information Figure S7 for a more detailed version of the calculation.  
11

12 424  
13  
14  
15  
16  
17  
18  
19  
20  
21  
22  
23  
24  
25  
26  
27  
28  
29  
30  
31  
32  
33  
34  
35  
36  
37  
38  
39  
40  
41  
42  
43  
44  
45  
46  
47  
48  
49  
50  
51  
52  
53  
54  
55  
56  
57  
58  
59  
60

425 **Table of Contents Graphic**

Black P



426